GRACE Gravity Data Constrain Ancient Ice Geometries and Continental Dynamics over Laurentia

M. E. Tamisiea, *et al.*

Science **316**, 881 (2007);
DOI: 10.1126/science.1137157

Science (print ISSN 0036-8075; online ISSN 1095-9203) is published weekly, except the last week in December, by the American Association for the Advancement of Science, 1200 New York Avenue NW, Washington, DC 20005.

decomposition reaction (no time for grain growth during seismic-fault motion). The process may be similar to the cases of intermediate- to deep-focus earthquakes, for which the formation of ultrafine reaction products may play a decisive role in earthquake generation (*28*). Other gouge materials have to undergo grain comminution to form ultrafine grains, which requires extra work in fault zones, resulting in higher friction. For slip on faults in Carrara marble, understanding friction between nanometer-scale particles seems to be a key for delineating the exact mechanisms of the dynamic weakening of faults.

Our results have important implications for earthquake geology and fault mechanics. Marked decomposition weakening may be a widespread phenomenon, because fault gouges commonly contain sheet silicate minerals that decompose even at lower temperatures than that for calcite decomposition, although thermal decomposition of sheet silicates may be followed by frictional melting (*29*). Also, thermally induced decomposition may leave geological evidence (other than pseudotachylytes) of seismic-fault slip, contrary to geologists' opinion that faults do not preserve a record of seismic slip, except for the small percentage of faults containing pseudotachylyte (*30*). Indeed, we have shown that coseismic decomposition of siderite produces a stable mineral, magnetite (*31*). Thus, the clear demonstration of thermal decomposition during seismic slip opens up a new series of investigations in integrated fault and earthquake studies.

References and Notes

1. C. H. Scholz, *The Mechanics of Earthquakes and Faulting* (Cambridge Univ. Press, New York, ed. 2, 2002).
2. M. D. Zoback *et al.*, *Science* **238**, 1105 (1987).
3. J. N. Brune, T. L. Henyey, R. F. Roy, *J. Geophys. Res.* **74**, 3821 (1969).
4. A. H. Lachenbruch, J. H. Sass, *J. Geophys. Res.* **85**, 6185 (1980).
5. R. H. Sibson, *Geophys. J. R. Astron. Soc.* **43**, 775 (1975).
6. A. Tsutsumi, T. Shimamoto, *Geophys. Res. Lett.* **24**, 699 (1997).
7. T. Hirose, T. Shimamoto, *J. Geophys. Res.* **110**, B05202 (2005).
8. T. Hirose, T. Shimamoto, *Bull. Seismol. Soc. Am.* **95**, 1666 (2005).
9. G. Di Toro, T. Hirose, S. Nielsen, G. Pennacchioni, T. Shimamoto, *Science* **311**, 647 (2006).
10. R. H. Sibson, *Nat. Phys. Sci.* **243**, 66 (1973).
11. A. H. Lachenbruch, *J. Geophys. Res.* **85**, 6097 (1980).
12. C. A. J. Wibberley, T. Shimamoto, *Nature* **436**, 689 (2005).
13. J. R. Rice, *J. Geophys. Res.* **111**, B05311 (2006).
14. D. L. Goldsby, T. E. Tullis, *Geophys. Res. Lett.* **29**, 1844 (2002).
15. G. Di Toro, D. E. Goldsby, T. E. Tullis, *Nature* **427**, 436 (2004).
16. K. Mizoguchi, T. Hirose, T. Shimamoto, E. Fukuyama, *Geophys. Res. Lett.* **34**, L01308 (2007).
17. C. B. Raleigh, M. S. Paterson, *J. Geophys. Res.* **70**, 3965 (1965).
18. T. Shimamoto, A. Tsutsumi, *Struct. Geol.* **39**, 65 (1994) (in Japanese with English abstract).
19. Materials and methods are available as supporting material on *Science* Online.
20. μ_p is the ratio of the highest shear stress to normal stress before the onset of weakening, and μ_{ss} is the ratio of steady-state shear stress to normal stress.
21. M. S. Paterson, T.-f. Wong, *Experimental Rock Deformation—The Brittle Field* (Springer-Verlag, Berlin, ed. 2, 2005).
22. W. A. Deer, R. A. Howie, J. Zussman, *An Introduction to the Rock Forming Minerals* (Longman Scientific and Technical, Harlow, UK, ed. 2, 1992).
23. Z. D. Sharp, J. J. Papike, T. Durakiewicz, *Am. Mineral.* **88**, 87 (2003).
24. The calculated bulk temperature (~850°C) on the sliding surface after 0.2 s appears to be consistent with the immediate decomposition after the onset of slip (*19*).
25. E. Tenthorey, S. F. Cox, *Geology* **31**, 921 (2003).
26. D. J. Andrews, Y. Ben-Zion, *J. Geophys. Res.* **102**, 553 (1997).
27. A. Tsutsumi, T. Shimamoto, in *Contemporary Lithosphertic Motion in Seismic Geology: Proceedings of the 30th International Geological Congress*, Y. Hong, Ed. (VNU Science Press, Leiden, Netherlands, 1997), pp. 223–232.
28. H. W. Green II, C. Marone, in *Plastic Deformation of Minerals and Rock*, S. Karato, H.-R. Wenk, Eds. (Mineralogical Society of America, Washington, DC, 2002), pp. 181–199.
29. J.-H. Ree, R. Han, T. Shimamoto, J. Kim, *Eos* **87**, S33A (2006).
30. D. S. Cowan, *J. Struct. Geol.* **21**, 995 (1999).
31. R. Han, T. Shimamoto, T. Hirose, J.-H. Ree, J. Ando, *Eos* **87**, S33A (2006).

32. The observations of the experimental specimens were made with the use of TEM (JEOL JEM-2010) at the Natural Science Center for Basic Research and Development of Hiroshima University and FE-SEM (JEOL JSM-7000F) at Geodynamics Research Center of Ehime University. This work was supported by the Brain Korea 21 Project of the Ministry of Education, Korea Research Foundation grant C00435 (100699), the Grant-in-Aid for Scientific Research, Japan Society for Promotion of Science (16340129 and 18340159), and the Center of Excellence Program for the 21st Century of Kyoto University, "Active Geosphere Investigation."

Supporting Online Material

www.sciencemag.org/cgi/content/full/316/5826/878/DC1
Materials and Methods
Figs. S1 to S4
References

10 January 2007; accepted 26 March 2007
10.1126/science.1139763

GRACE Gravity Data Constrain Ancient Ice Geometries and Continental Dynamics over Laurentia

M. E. Tamisiea,[1]*† J. X. Mitrovica,[2] J. L. Davis[1]

The free-air gravity trend over Canada, derived from the Gravity Recovery and Climate Experiment (GRACE) satellite mission, robustly isolates the gravity signal associated with glacial isostatic adjustment (GIA) from the longer–time scale mantle convection process. This trend proves that the ancient Laurentian ice complex was composed of two large domes to the west and east of Hudson Bay, in accord with one of two classes of earlier reconstructions. Moreover, GIA models that reconcile the peak rates contribute ~25 to ~45% to the observed static gravity field, which represents an important boundary condition on the buoyancy of the continental tectosphere.

The similarity between the geometry of the free-air gravity anomaly (FAGA) over Laurentia (*1*) and the perimeter of the ancient ice complex that covered the region led to a long-held view that the perturbation largely reflected incomplete GIA in response to the ice age (*1–4*). In this case, the seismic high-velocity anomaly underlying the continent (*5*) would be interpreted as a neutrally buoyant, chemically distinct continental root, in accord with the tectosphere hypothesis (*6*). In contrast, forward analyses of GIA and/or mantle convection aimed at fitting the peak anomaly (*7–9*) have concluded that GIA is responsible for only ~10 to ~30% of the total signal. In this scenario, the seismic anomaly would be associated with active downwelling flow that drives a dynamic depression, and gravity low, on the overriding craton. Simons and Hager (*10*) have, on the basis of GIA modeling combined with an analysis of the spatio-spectral content of the Laurentian gravity field, proposed an intermediate scenario in which GIA and convection contribute roughly equally to the observed signal.

The characteristic time scale of GIA (a few thousand years) is orders of magnitude shorter than that of convective flow. Accordingly, Mitrovica and Peltier (*4*) suggested that consideration of the time rate of change of the gravity field would, when it became available, provide a robust method for isolating the GIA signal. The trend field would also provide finer spatial resolution of ice-sheet history than the static field. Observational constraints on gravity trends from land-based surveys in Hudson Bay exist (*11*, *12*), but these are too sparse to accurately constrain the regional (and peak) GIA signal. Recently, measurements obtained by the GRACE satellite mission (*13*) have reached sufficient time span to yield useful constraints on regional gravity trends. Our goal is to make use of the GRACE data to constrain the GIA signal and thus test the suite of published models for the dynamics of the Laurentian craton. We also use the GRACE-derived maps of gravity rates to address a century-long debate concerning the geometry of late Pleistocene ice cover over the region.

We use monthly Center for Space Research (CSR) RL01 GRACE solutions for the geoid,

[1]Harvard-Smithsonian Center for Astrophysics, 60 Garden Street, Mail Stop 42, Cambridge, MA 02143, USA. [2]Department of Physics, University of Toronto, 60 St. George Street, Toronto, ON M5S 1A7, Canada.

*Present address: Proudman Oceanographic Laboratory, 6 Brownlow Street, Liverpool L3 5DA, UK.
†To whom correspondence should be addressed. E-mail: mtamisiea@cfa.harvard.edu

spanning April 2002 to April 2006. Our analysis procedure (*14*) adopts a truncation at spherical harmonic degree and order (l and m, respectively) of 70, applies standard approaches to smoothing (Gaussian with a 500-km radius) and destriping the solutions to reduce satellite errors, and yields estimates for parameters governing the in- and out-of-phase annual, trend, and constant terms and their errors. We calculate the geoid height anomaly rates from each solution on a 1° by 1° grid. The result, over Laurentia, is shown in Fig. 1.

Previous applications of GRACE data have focused on rates associated with hydrological processes (*13*), and the standard approach in such cases is to convert the geoid height rates to changes in equivalent water thickness. With respect to the spherical harmonic expansion, each term is multiplied by $2l + 1$ (*15*), thus accentuating higher degree and order terms (and their associated error). The signal associated with GIA is largely due to the motion of mass within the Earth's crust and mantle, as opposed to variations of surface and groundwater mass. In this application, or indeed in studies of surface observations related to mantle convection, geoid rates are commonly converted to trends in the FAGA. In this case, a multiplicative factor of $l - 1$ is applied (*16*) to each term in the spherical harmonic expansion, which acts to shift power to shorter wavelengths. Smaller-scale features in the FAGA are therefore emphasized relative to those in the geoid.

Our GRACE-derived map of the FAGA trend over Laurentia (Fig. 2A and the associated error estimate in fig. S1A) unambiguously indicates that the ancient ice complex that once covered the region had a multidomal structure. Specifically, deglaciation centers are apparent in regions to the west (Keewatin) and east (northern Quebec) of Hudson Bay. The broad-scale geometry of the Laurentide Ice Sheet at the Last Glacial Maximum has been the source of long-standing debate [see (*17*) for a review of early work]. Before the mid-20th century, reconstructions of Laurentide ice cover generally included ice domes over Keewatin and northern Quebec, but this view was superseded by the monodomal model advocated by Flint (*18*) on the basis of an analysis of gravity data. Subsequent studies, in particular the detailed geomorphological analysis of Dyke and Prest (*19*), returned to the multidomal (i.e., ice domes over Keewatin, northern Quebec, and the Foxe Basin just south of Baffin Island) model, although the ICE-3G (*17*) and ICE-4G (*20*) global ice-sheet reconstructions, based on both geological and geophysical data, were once again characterized by a largely monodomal Laurentian complex. A recent revision to these global models, ICE-5G (*21*), motivated in part by crustal motion data in Yellowknife and ground-based gravity measurements along a transect including the west coast of Hudson Bay (*11*), involved a major ice dome over Keewatin and a smaller ice center in northern Quebec, in qualitative accord with the Dyke and Prest (*19*) reconstruction. Our results strongly support the multidomal Laurentide ice geometry advocated by Dyke and Prest (*19*) and allow us to reject the monodomal model.

GIA is not the only process contributing to the observed rate fields. Interannual variations in hydrology, mass loss from Greenland Ice Sheet and Alaskan glacier fields, and errors in the ocean model of Hudson Bay could all contribute to the observed signal. In an attempt to account for hydrology, we have calculated the rate over the same time period from the Global Land Data Assimilation System (GLDAS)/Noah hydrology data set (*14*, *22*). This correction is small in terms of the total signal observed in the region, but it slightly decreases the local maximum value of the observed FAGA rate west of Hudson Bay and moves the location of this peak rate farther north (Fig. 2B). In an attempt to reduce the contamination from mass loss of the ice fields, this paper focuses on comparisons of forward predictions of GIA with the observed FAGA in a region bounded by longitudes 110°W to 85°W and latitudes 50°N to 70°N (indicated by the area within the black line in Fig. 2B). Possible errors due to ocean variability in Hudson Bay are part of an ongoing study.

We adopt the following procedure to estimate the contribution of GIA to the static FAGA over Laurentia. First, we use standard numerical simulations of the GIA process to generate a model (or set of models) that provides a good fit to the rate map in Fig. 2B. We next use this model to predict the static FAGA and then compare this prediction to the GRACE-derived static field within the bounded region. In all cases, we apply the same smoothing, destriping, and harmonic truncation to the GIA model predictions that were used to analyze the GRACE observations (*14*).

Our GIA predictions are based on spherically symmetric, self-gravitating Maxwell viscoelastic Earth models with elastic structure given by the Preliminary Reference Earth Model (*23*). We assume an elastic lithosphere of 120-km thickness (the predictions are insensitive to reasonable variations in this choice) and a radial viscosity profile characterized by isoviscous upper and lower mantle (UM and LM) regions. The boundary between these regions is taken at 670-km depth, and the viscosities above and below this interface are free parameters denoted by ν_{UM} and ν_{LM}, respectively. We use the global ICE-5G ice history (*21*) and solve for a gravitationally self-consistent ocean load.

Figure 3 shows the reduced χ^2 misfit between predictions of the geoid and FAGA rate fields over Laurentia and the associated GRACE observations [Fig. 1 (with the hydrological signal removed) and Fig. 2B, respectively]. Good fits (*24*) to the data are generally obtained for models with ν_{LM} values between 2.5×10^{21} and 4×10^{21} Pa s and ν_{UM} values between 3×10^{20} and 1×10^{21} Pa s. A second set of models characterized by ν_{UM} above 6×10^{20} Pa s and

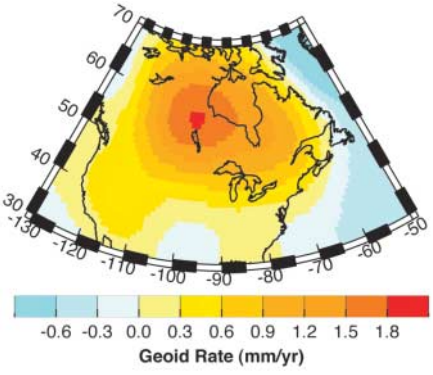

Fig. 1. Observed time rate of change of the geoid over Laurentia from CSR RL01 GRACE solutions from April 2002 to April 2006.

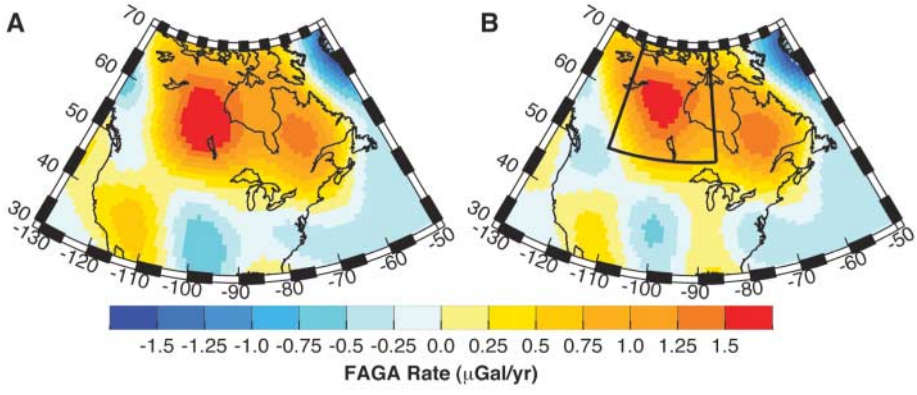

Fig. 2. (**A**) Rate of change of the FAGA from CSR RL01 GRACE solutions from April 2002 to April 2006. (**B**) Same as (A) but with an estimate of the hydrological contribution derived from the GLDAS/Noah data set (*22*) removed. The thick black line encloses the region used for the comparison of the forward GIA models with the observed fields. This region was chosen in order to limit contamination from ongoing ice mass variations in Greenland, Alaska, and British Columbia, as well as hydrological mass variations across the rest of the North American continent.

ν_{LM} greater than 3×10^{22} Pa s also yields relatively low χ^2 values. Two sets of solutions of this type are common in studies of present-day GIA observations. A weak lower mantle associated with the first class of models initially adjusts quickly and thus reaches close to equilibrium since the end of the deglaciation, whereas a stronger lower mantle (in the second class of models) adjusts slowly throughout the loading cycle. We can rule out the higher mantle viscosity models on the basis of independent analyses of postglacial decay times in the Hudson Bay region (*20*, *25*). The minimum reduced χ^2 misfit, for the FAGA rate (Fig. 3B) observation, is obtained by the model with $\nu_{UM} = 8 \times 10^{20}$ Pa s and $\nu_{LM} = 3 \times 10^{21}$ Pa s.

Next, we turn to the static FAGA field. In this case, our GRACE-derived (Fig. 4A) estimate is based on the CSR GGM02S solution (*26*). Note that this static field shows a single large anomaly with peak amplitude of −34 mGal (where 1 Gal = 10^{-2} m s^{-2}) centered over Hudson Bay and, as discussed above, a geometry that is less reflective of the morphology of the ancient ice complex that covered the region. Our next step is to predict the static FAGA field due to GIA with the use of the same Earth model that best fits the FAGA rate (*27*). Figure 4B shows the residual field generated by removing this GIA prediction from the observed static field (Fig. 4A). Classically, peak estimates of the GIA prediction and the static FAGA observation, which do not necessarily occur at the same location, have been compared to determine the relative contribution of GIA to the observed field. The application of this procedure indicates a GIA contribution of ~38% (or –13 mGal) to the observed peak.

As noted, a range of GIA models provides similar fits to the GRACE-derived rates (Fig. 3). Therefore, we repeated the above analysis for a large suite of models within this range and, in each case, we computed the GIA contribution to the static FAGA. In addition, we also considered the impact on this contribution (and on the preferred set of models) of errors in the hydrology model and variations in the parameters governing the GRACE data analysis [e.g., destriping and Gaussian smoothing (*14*)]. These tests mapped out a possible range in the GIA contribution to the static FAGA field of ~25 to ~45%. Thus, the continental root beneath Laurentia is contributing, via a convectively supported dynamic depression of the craton, to the FAGA field. This range is intermediate as compared to estimates by Simons and Hager (*10*), who argued for a 50% contribution from GIA, and other studies that have concluded that GIA is a minor contributor to the static field (*7*–*9*). In any case, although chemical heterogeneity in the continental root beneath Laurentia is compensating for thermal buoyancy, the cancellation implied by the tectosphere hypothesis is not supported by our analysis of the GRACE-derived gravity field.

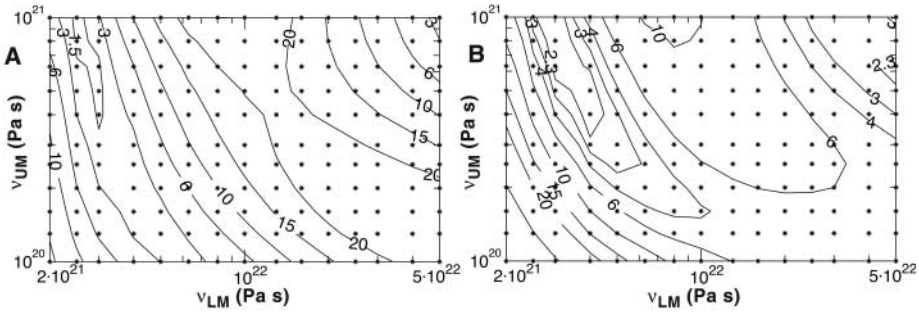

Fig. 3. (**A**) Reduced χ^2 residual between GIA predictions of the geoid rate and the observed field (Fig. 1) on a 1° by 1° grid within the region bounded by the thick black line in Fig. 2B. The GIA models are distinguished on the basis of the adopted ν_{UM} and ν_{LM} values, and the grid of dots indicates the set of models used to generate the contour lines. (**B**) Same as in (A) but for the FAGA rate field.

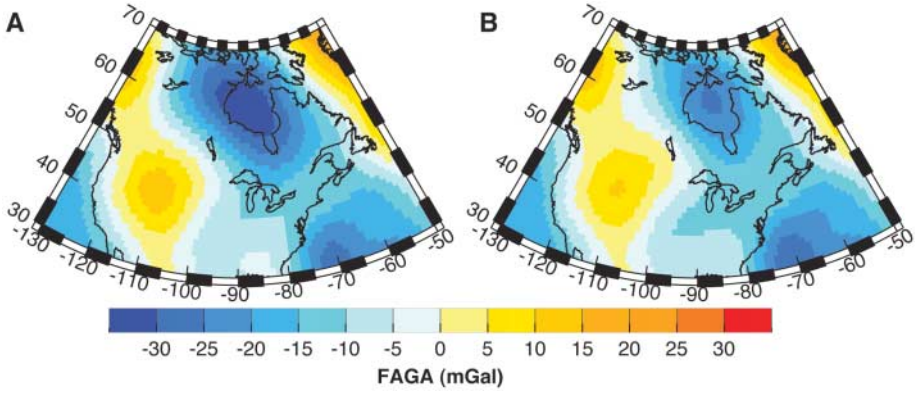

Fig. 4. (**A**) Static FAGA field over Laurentia derived from the CSR GGM02S GRACE solution (*26*). A destriping algorithm (*14*) was not applied to generate this field. (**B**) Same as (A) but with a "preferred" GIA prediction removed. The GIA prediction is based on an Earth model with a 120-km-thick lithosphere, a ν_{UM} value of 8×10^{20} Pa s, and a ν_{LM} value of 3×10^{21} Pa s.

References and Notes

1. R. I. Walcott, *Can. J. Earth Sci.* **7**, 716 (1970).
2. L. M. Cathles, *The Viscosity of the Earth's Mantle* (Princeton Univ. Press, Princeton, NJ, 1975).
3. P. Wu, W. R. Peltier, *Geophys. J. R. Astron. Soc.* **74**, 377 (1983).
4. J. X. Mitrovica, W. R. Peltier, *J. Geophys. Res.* **94**, 13651 (1989).
5. J. Ritsema, H. J. van Heijst, J. H. Woodhouse, *Science* **286**, 1925 (1999).
6. T. H. Jordan, *Rev. Geophys. Space Phys.* **13**, 1 (1975).
7. W. R. Peltier, A. M. Forte, J. X. Mitrovica, A. M. Dziewonski, *Geophys. Res. Lett.* **19**, 1555 (1992).
8. T. S. James, *Geophys. Res. Lett.* **19**, 861 (1992).
9. G. Pari, W. R. Peltier, *J. Geophys. Res.* **101**, 28105 (1996).
10. M. Simons, B. H. Hager, *Nature* **390**, 500 (1997).
11. A. Lambert *et al.*, *Geophys. Res. Lett.* **28**, 2109 (2001).
12. A. Lambert, N. Courtier, T. S. James, *J. Geodyn.* **41**, 307 (2006).
13. B. D. Tapley, S. Bettadpur, J. C. Ries, P. F. Thompson, M. M. Watkins, *Science* **305**, 503 (2004).
14. Materials and methods are available as supporting material on *Science* Online.
15. J. Wahr, M. Molenaar, F. Bryan, *J. Geophys. Res.* **103**, 30205 (1998).
16. G. D. Garland, *Introduction to Geophysics: Mantle, Core, and Crust* (Saunders, Philadelphia, ed. 2, 1979).
17. A. M. Tushingham, W. R. Peltier, *J. Geophys. Res.* **96**, 4497 (1991).
18. R. F. Flint, *Glacial Geology and the Pleistocene Epoch* (Wiley, New York, 1947).
19. A. S. Dyke, V. K. Prest, *Geogr. Phys. Quat.* **41**, 237 (1987).
20. W. R. Peltier, *Rev. Geophys.* **36**, 603 (1998).
21. W. R. Peltier, *Annu. Rev. Earth Planet. Sci.* **32**, 111 (2004).
22. M. Rodell *et al.*, *Bull. Am. Meteorol. Soc.* **85**, 381 (2004).
23. A. M. Dziewonski, D. L. Anderson, *Phys. Earth Planet. Inter.* **25**, 297 (1981).
24. If we assume that we can apply a standard *F* test to the data, then a reasonable 95% confidence limit for χ^2 would be 1.5 and 2.3 for Fig. 3, A and B, respectively. We have conservatively taken the degrees of freedom in the problem to be 10% of the total number of grid points.
25. J. X. Mitrovica, A. M. Forte, *J. Geophys. Res.* **102**, 2751 (1997).
26. B. Tapley *et al.*, *J. Geodesy* **79**, 467 (2005).
27. The number of glacial cycles used in the calculation will affect predictions of the static FAGA caused by GIA. Thus, we have included three complete glacial cycles before the last cycle specified by ICE-5G. The inclusion of these cycles will have little impact on the estimates of present-day rates.

28. This work was supported under the National Aeronautics and Space Administration (grant number NNG04GF09G), the Natural Sciences and Engineering Research Council of Canada, Geomatics for Informed Decisions, and the Canadian Institute for Advanced Research. We thank E. Hill, K. Latychev, S. Swenson, I. Velicogna, J. Wahr, and W. van der Wal for useful conversations and two anonymous reviewers for helpful suggestions for improving the manuscript.

Supporting Online Material

www.sciencemag.org/cgi/content/full/316/5826/881/DC1
Materials and Methods
Figs. S1 and S2
References

3 November 2006; accepted 28 March 2007
10.1126/science.1137157